Eur Biophys J (2011) 40:661–671
DOI 10.1007/s00249-011-0669-4

ORIGINAL PAPER

Internal motions of actin characterized by quasielastic neutron scattering

Satoru Fujiwara · Marie Plazanet · Fumiko Matsumoto · Toshiro Oda

Received: 23 August 2010 / Revised: 28 December 2010 / Accepted: 3 January 2011 / Published online: 20 January 2011

Abstract Quasielastic neutron scattering (QENS) experiments were carried out on powders of F-actin and G-actin hydrated with D_2O to characterize the internal dynamics on the picosecond time scale and the Ångstrom length scale. To investigate the effects of hydration, the measurements were done on samples at hydration ratio (h) of 0.4 (mg D_2O/mg protein), containing only the first layer of hydration water, and at $h = 1.0$, containing more layers of water. The QENS spectra, obtained from the measurements at two energy resolutions of 110 and 15 μeV, indicated that the internal motions of both F-actin and G-actin have distributions of motions with distinct correlation times and amplitudes. Increasing hydration changes relative populations of these distinct motions. The effects of hydration were shown to be different between F-actin and G-actin. Elastic incoherent neutron scattering measurements provided the concerted results. The observed effects were interpreted in terms of the dynamical heterogeneity of the actin molecule: in G-actin, more surface loops become flexible and undergo diffusive motions of large amplitudes, whereas in F-actin the molecular interactions that keep the polymerized state suppress the large motions of the surface loops involved with polymerization so that the population of atoms undergoing large motions can increase only to a lesser degree.

Keywords Quasielastic neutron scattering · Actin · Hydration · Elastic incoherent neutron scattering · Mean square displacement · Flexibility of actin

S. Fujiwara (✉) · F. Matsumoto
Quantum Beam Science Directorate, Japan Atomic Energy Agency, 2-4 Shirakata-Shirane, Tokai-mura, Naka-gun, Ibaraki 319-1195, Japan
e-mail: fujiwara.satoru@jaea.go.jp

M. Plazanet
Laboratoire de Spectrométrie Physique, Université Joseph Fourier de Grenoble and CNRS (UMR5588), BP87, 38402 Saint Martin d'Hères Cedex 9, France

T. Oda
RIKEN SPring-8 Center, RIKEN Harima Institute, 1-1-1 Kouto, Sayo-gun, Hyogo 679-5148, Japan

Introduction

Actin is one of the most abundant proteins in eukaryotic cells and carries out various cellular functions related to cell motility and morphology including cell locomotion, cell division, and transport of intracellular organelles (Carlier and Pantaloni 1997; Pollard et al. 2000). The actin monomers (G-actin) polymerize to form a helical polymer (F-actin). This polymerization-depolymerization process, controlled through interactions with various actin-binding proteins, plays crucial roles in a variety of functions of actin. F-actin has been shown to exhibit various degrees of flexibility depending on its environmental conditions (Ishiwata and Fujime 1972; Janmey et al. 1990; Orlova and Egelman 1993; Isambert et al. 1995; Rebello and Ludescher 1998). This modulation of flexibility of F-actin has been suggested as important in expressing multiple functions (Ishiwata and Fujime 1972; Orlova and Egelman 1993; Isambert et al. 1995). Elucidation of the mechanism of multi-functions of actin thus requires understanding of the flexibility of F-actin.

Flexibility arises from the motions of F-actin that occur at various levels, from large scale motions of F-actin as a whole on a millisecond time scale and a μm length scale, through relative motions of the actin protomers and subdomain motions within the actin protomers, down to

thermal fluctuations of polypeptide chains and their side chains on a picosecond time scale and an Ångstrom length scale. Well-accepted knowledge that thermal fluctuations of atoms within a protein are crucial for conformational changes of the protein to occur, and hence function (Zaccai 2000), implies that these motions at different levels are closely related to each other. Understanding of the flexibility of F-actin thus requires characterizing this hierarchy of dynamics.

Towards this ultimate purpose, we have started to investigate the internal dynamics of the actin protomers in F-actin with neutron scattering. Neutron scattering provides unique tools to directly measure the internal dynamics of biological macromolecules (Smith 1991). Because of the large incoherent scattering cross-section of hydrogen atoms compared to other atoms found in proteins and solvents, elastic or quasi-elastic incoherent neutron scattering arise predominantly from the hydrogen motions. The measurements thus monitor the average individual dynamics of hydrogen atoms within the protein. High abundance (up to 50%) and nearly homogeneous distribution of hydrogen atoms in the protein make it possible to characterize the internal dynamics of the protein in a global manner. In a previous study (Fujiwara et al. 2008), we have employed elastic incoherent neutron scattering (EINS). The EINS experiments provide estimation of the atomic mean square displacement that is principally due to hydrogen atoms, the motions of which reflect those of the side chains and backbone atoms to which they are bound (Smith 1991). Temperature dependence of this mean square displacement provides a measure of the flexibility of the protein. We performed the EINS experiments of the hydrated powders of F-actin and G-actin, containing one layer of hydration water, and found that behavior of the mean square displacements is different between G-actin and F-actin, such that G-actin is "softer" than F-actin, and that this different behavior observed is ascribed to the differences in dynamical heterogeneity between F-actin and G-actin.

Here, quasi-elastic neutron scattering (QENS) was employed to further characterize the internal dynamics of actin. This technique provides information on correlation times and geometry of the averaged atomic motions, and has been applied to a variety of systems of biological macromolecules, from proteins and their hydration water to bacterial cells (Doster et al. 1989; Bellissent-Funel et al. 1992; Fitter et al. 1996, 1998; Receveur et al. 1997; Fitter 1999, 2003; Zanotti et al. 1999, 2006; Pérez et al. 1999; Paciaroni et al. 1999; Dellerue and Bellissent-Funel 2000; Bu et al. 2000, 2001; Bon et al. 2002; De Francesco et al. 2004; Bastos et al. 2004; Caronna et al. 2005; Pieper et al. 2007, 2008a, b; Tehei et al. 2007; Gasper et al. 2008; Köper et al. 2008; Jasnin et al. 2008; Stadler et al. 2008). We prepared powder samples of F-actin and G-actin hydrated with D_2O, and performed the QENS experiments of these samples. Particular attention was paid to the effects of hydration. Since the proteins usually function in aqueous environments containing more water than one layer of hydration water, the way in which water outside of the hydration layer might affect the internal dynamics of the protein is important in understanding the multi-functions of actin. We thus aimed at characterizing the internal dynamics of F-actin and G-actin under two different conditions of hydration: samples containing only the first hydration water, and samples containing more layers of water in addition to the first hydration water. To do this, we prepared the D_2O-hydrated powder samples with different degrees of hydration ratio corresponding to these conditions: the sample at the hydration ratio (h) of 0.4 (g D_2O/g protein) and that at $h = 1.0$. The QENS measurements on these samples detected different effects of hydration on the internal protein dynamics between F-actin and G-actin. The EINS measurements on the same samples provided consistent results.

Materials and methods

Sample preparation

The hydrated powder samples of F-actin and G-actin at $h = 0.4$ were prepared exactly as previously described (Fujiwara et al. 2008). Briefly, actin was purified from acetone powder of chicken breast muscle according to the standard procedure (Spudich and Watt 1971). F-actin was prepared by polymerization of the actin molecules in the solution containing 60 mM KCl, 2 mM $MgCl_2$, 0.1 mM $CaCl_2$, 0.2 mM ATP, and 2 mM Tris–HCl (pH 8.0). For the preparation of G-actin, the actin molecule was labeled with the fluorescent probe tetramethyl-rhodamine-5-maleimide (TMR), which inhibits polymerization of the actin molecules (Otterbein et al. 2001). This TMR-labeled actin, suspended in the solution containing 0.1 mM $CaCl_2$, 0.2 mM ATP, and 2 mM Tris–HCl (pH 8.0), was used as G-actin. Note that TMR does not contribute QENS or EINS spectra significantly because of small number of hydrogen atoms in TMR compared to the actin molecule (23 in TMR and 2273 in the actin molecule). Note also that comparison of the temperature factors, which can be a measure of the dynamics, of the crystal structure of the TMR-labeled actin (PDB code: 1J6Z, Otterbein et al. 2001) and that of the unlabeled actin (PDB code: 2HF3, the structure solved at a similar resolution to 1J6Z, Rould et al. 2006) showed that they have similar distributions along the residue numbers (data not shown). This implies that TMR does not change the dynamics of the actin molecule significantly.

Purified F-actin and G-actin were suspended in appropriate solutions in D_2O, concentrated, and dried in D_2O atmosphere so that the signals from the proteins were dominant. The samples at $h = 1.0$ were prepared by adding appropriate amounts of D_2O to the powders at $h = 0.4$ because the equilibrium with D_2O atmosphere did not bring the samples to such a high value of the hydration ratio. The precise hydration ratios of F-actin were 0.38 and 0.97 for the samples denominated by $h = 0.4$ and $h = 1.0$, respectively. The hydration ratios of G-actin were 0.36 and 1.16 for the samples denominated by $h = 0.4$ and $h = 1.0$, respectively. Structural integrity of F-actin in the powder samples was checked by X-ray diffraction experiments, performed at the small-angle scattering station BL-45XU-SAXS (Fujisawa et al. 2000) at SPring8, Harima, Japan. The diffraction patterns of the F-actin powders (data not shown) showed a peak at the position corresponding to the strong layer-lines at 59 and 51 Å in the fiber diffraction pattern of F-actin (the intensity distributions of the two layer-lines were fused into one rather broad peak because of spherical averaging), as found in the solution X-ray scattering pattern of F-actin (Matsudaira et al. 1987) and the diffraction pattern of the dried "thin-films" of F-actin (Astbury et al. 1947). This implies that the structural integrity of F-actin was maintained during the drying process. On the other hand, the patterns of G-actin powders did not show such peaks, indicating that polymerization did not occur on these samples.

Quasielastic neutron scattering experiments

The QENS experiments were performed on the disk chopper time-of-flight spectrometer IN5 at the Institut Laue-Langevin (ILL), Grenoble, France. The spectra were measured using incident neutrons of a wavelength of 5 Å at energy resolution of 110 μeV. The measurements were also done using incident neutrons of a wavelength of 10 Å at energy resolution of 15 μeV. The measured ranges of the momentum transfer, Q ($=4\pi\sin\theta/\lambda$, where 2θ denotes scattering angle and λ denotes the wavelength of incident neutrons), were between 0.45 and 2.1 $Å^{-1}$ for the measurements at 110 μeV, and between 0.24 and 1.0 $Å^{-1}$ for the measurements at 15 μeV, respectively. The energy resolutions of 110 and 15 μeV correspond to the motions faster than ~6 ps and ~44 ps, respectively. The measured time-of-flight spectra were normalized using the vanadium standard, corrected for transmission, subtracted the contribution from the sample cell, and transformed into the energy spectra. Data reduction was done with the ILL software package LAMP (http://www.ill.fr/data_treat/lamp/lamp.html).

The measured QENS spectra can be approximated by the following equation:

$$S(Q,\omega) = \mathrm{DW}(Q) \times \exp(-\hbar\omega/2k_BT) \times \left[(A_0(Q)\delta(\omega) + \sum_{i=1}^{N} A_i(Q)L_i(\omega,\Gamma_i)) \otimes R(Q,\omega) \right] + B(Q), \quad (1)$$

where $\hbar\omega$ is the energy transfer, $\mathrm{DW}(Q)$ denotes the Debye–Waller factor which represents the vibrational motions, and $\exp(-\hbar\omega/2k_BT)$ is the detailed balance factor. The terms in the bracket represent diffusive motions, where $A_0(Q)\delta(\omega)$ denotes the elastic component with $A_0(Q)$ being the fractional intensity and $\delta(\omega)$ the delta-function, and $A_i(Q)$ is the fractional intensity of the i-th Lorentzian $L_i(\omega, \Gamma_i)$ $(=(1/\pi) \times (\Gamma_i/(\Gamma_i^2 + \omega^2))$, where Γ_i is the half width at half maximum of this Lorentzian) (Bee 1988). Since the spectra are broadened by the resolution function, the terms representing the diffusive motions are convoluted by the resolution function, $R(Q,\omega)$. $\otimes$ denotes the convolution operation, and $B(Q)$ is the background. N is the number of Lorentzians required to describe the measured spectra. A small value of this number is usually sufficient because of the finite energy resolution and the statistics of the data. As shown below, the equation containing two Lorentzians ($N = 2$) fits well with the measured spectra. Information on the averaged motions can be obtained from these Lorentzians. The fitting of the measured spectra with Eq. 1 was done using the QENS_FIT routine in the package LAMP.

Elastic incoherent neutron scattering experiments

The EINS experiments were carried out on the backscattering spectrometer IN16 at the ILL, at an energy resolution of 0.9 μeV. The measurements of the samples at $h = 0.4$, previously published, were done in the temperature range between 20 and 300 K as described (Fujiwara et al. 2008). On the other hand, the new measurements of the samples at $h = 1.0$ were done in the temperature range between 280 and 300 K to avoid possible ice formation in the samples. The data were collected during a linear increase in temperature with the heating rate of 0.17 K/min. The data were corrected for scattering arising from the sample holder, and normalized by the intensity at the lowest temperature, T_{std} (the average intensity between 20 and 50 K was used as a standard here). Note that for the data of the samples at $h = 1.0$, the intensity was normalized by the intensity of the corresponding samples at $h = 0.4$. This is based on the assumption that at low temperature, where only the harmonic oscillation occurs, the behavior of the protein is the same regardless of the hydration, and that the signal arising from the additional water is negligible. Logarithm of this normalized intensity

was plotted against Q^2, and fit by a straight line, from the slope of which the mean square displacement, $<u^2>$, could be estimated. Because the intensities were normalized by that at T_{std}, the extracted value of $<u^2>$ at each temperature, T, corresponds to $<u^2(T)> - <u^2(T_{std})>$. The fitting ranges of these linear fits were selected so that the criterion for the Gaussian approximation ($<u^2> Q^2 < \sim 2$) strictly holds (Réat et al. 1997). We call this fitting range here the Guinier region, in analogy to small-angle scattering (Guinier and Fournet 1955). The linear fits were also performed to the Q-range larger than $Q^2 = 1.5$ Å^{-2} (the high-Q region), as done in the previous report (Fujiwara et al. 2008).

Results

QENS measurements

The QENS measurements were performed on the D_2O-hydrated powders of F-actin at $h = 0.4$ and 1.0, and G-actin at $h = 0.4$ and 1.0. Figure 1a and b shows examples of QENS spectra: the spectrum of F-actin at $h = 0.4$ at the temperature $T = 296$ K and that of F-actin at $h = 1.0$ at the temperature $T = 301$ K, for $Q = 2.03$ Å^{-1}, measured at the energy resolution of 110 μeV. In these figures, the results of the fits with Eq. 1 containing one or two Lorentzians are also plotted. As shown in the residuals of the fits in the lower panels in Fig. 1a and b and in the reduced-χ^2 values of the fits in Fig. 1c and d, the equation containing two Lorentzians consistently provided better fits than that containing a single Lorentzian. The addition of a third Lorentzian component did not provide significant improvement to the fit and only appeared as overfitting. Such results were consistently observed for all the spectra obtained. This implies that the internal motions of both F-actin and G-actin contain, on average, motions with two distinct correlation times. For each resolution, we refer to the narrow Lorentzian (corresponding to slower motions) by LZ1 and to the wider one by LZ2 (corresponding to faster motions). Note that, as shown below in Fig. 2, the half-width at half maximum, or Γ, value of LZ1 may be narrower than that of the resolution function in some cases. It is indeed widely accepted that a broadening of about 10% of the resolution width can be detected by QENS if the statistics are good enough (Pérez et al. 1999; Gasper

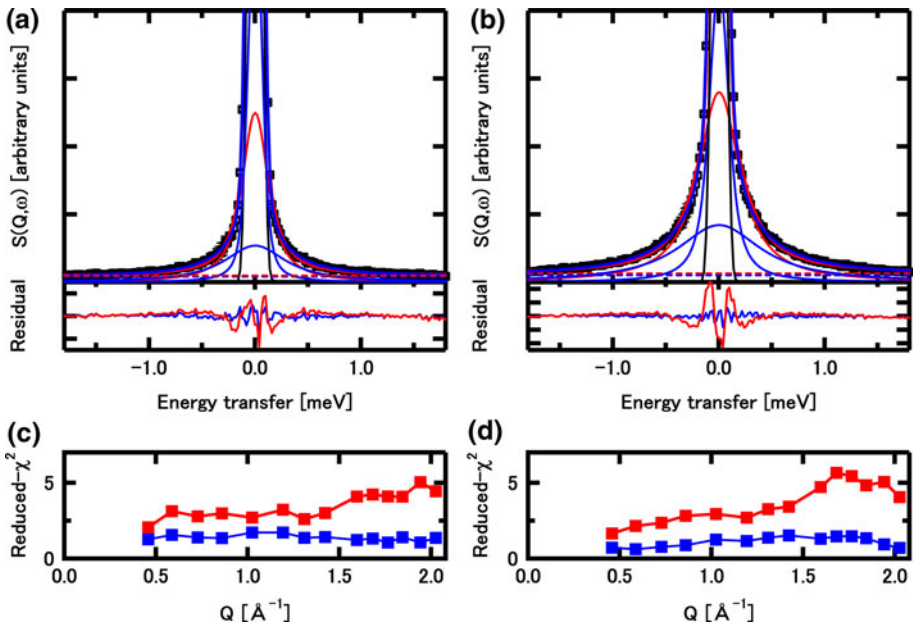

Fig. 1 Examples of quasielastic neutron scattering spectra $S(Q,\omega)$. The spectra of **a** F-actin at $h = 0.4$ at the temperature $T = 296$ K and of **b** F-actin at $h = 1.0$ at temperature $T = 301$ K, at $Q = 2.03$ Å^{-1}, measured at the energy resolution of 110 μeV, are shown. In the *upper panels*, *open squares* denote the data points, *solid lines* in *black* denote the resolution functions, *thick solid lines* in *blue* denote the total fits by Eq. 1 containing two Lorentzians, *thin solid lines* in *blue* were the two Lorentzian components, *dashed lines* in *blue* denote the background component of the fits, *thick solid lines* in *red* denote the total fits by Eq. 1 containing single Lorentzian, *thin solid lines* in *red* denote the Lorentzian component, and the *dashed lines* in *red* denote the background component of the fits. The *error bars* of the data points are within *symbols*. In the *lower panels*, the residuals of the fits are shown. The *lines* in *blue* denote the residuals for the fit with the equation containing the two Lorentzians while the *lines* in *red* denote the residuals for the fit with the equation containing the single Lorentzian. **c** Reduced-χ^2 of the fits to the data of F-actin at $h = 0.4$ at the temperature $T = 296$ K. **d** Reduced-χ^2 of the fits to the data of F-actin at $h = 1.0$ at the temperature $T = 301$ K. *Filled squares* in *blue* and in *red* are the values of the fit with the equation containing two Lorentzians and those containing single Lorentzian, respectively

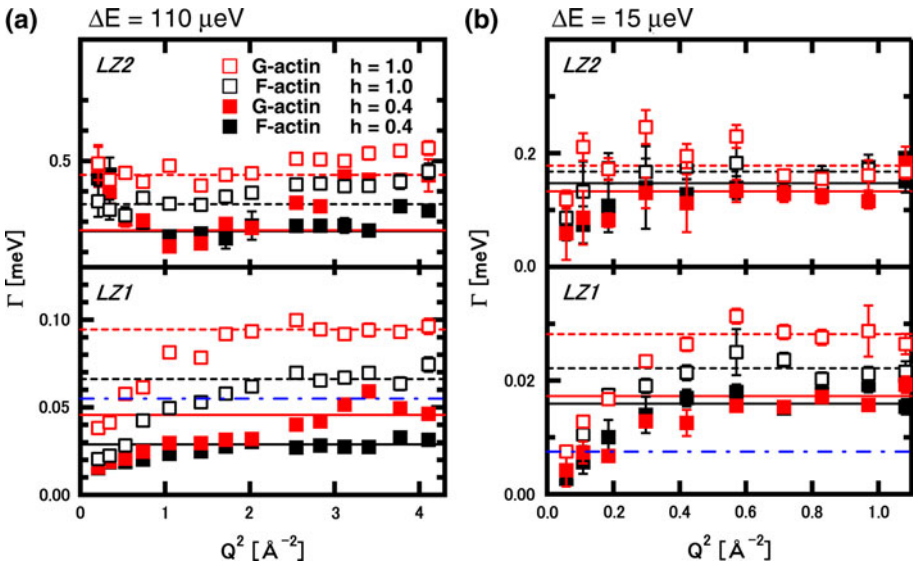

Fig. 2 Q-dependences of half width at half-maximum, Γ, of the Lorentzians with narrow widths (LZ1) and large widths (LZ2). **a** The results of the fits to the data of the measurements at the energy resolution (ΔE) of 110 μeV are shown. The temperatures of the measurements were 296, 301, 301, and 305 K, for F-actin at $h = 0.4$, F-actin at $h = 1.0$, G-actin at $h = 0.4$, and G-actin at $h = 1.0$, respectively. **b** The results to the data of the measurements at ΔE of 15 μeV. The temperatures of the measurements were 301, 299, and 298 K, for F-actin at $h = 0.4$ and 1.0, G-actin at $h = 0.4$, and G-actin at $h = 1.0$, respectively, here. *Filled squares* in *black*, *filled squares* in *red*, *open squares* in *black*, and *open squares* in *red* denote the results of F-actin at $h = 0.4$, G-actin at $h = 0.4$, F-actin at $h = 1.0$, and G-actin at $h = 1.0$, respectively. The *error bars* are within *symbols* if not shown. The *dashed*-and-*dotted lines* denote the level of half-width at half maximum of the resolution functions. The *dashed lines* indicate the plateau value in each panel. The plateau regions of LZ2 for the measurement at 110 μeV were assumed to be between 0.5 and 2.1 $Å^{-2}$. On the other hand, LZ1 approached asymptotically to the plateau region between 2.5 and 4.2 $Å^{-2}$. The plateau regions of LZ2 and LZ1 in the high-Q regions for the measurements at 15 μeV were assumed to be between 0.6 and 1.1 $Å^{-2}$

et al. 2008). The Γ values here have error bars small enough to detect such a broadening. The measurements were done at three temperature points between ∼280 and ∼300 K. Temperature dependence of the Γ values were, however, not significant in this temperature range (data not shown). The results of the data obtained at around 300 K are thus described below as representative.

Figure 2 summarizes the Q-dependences of the Γ values of the Lorentzians of F-actin and G-actin. The results of the measurements at the energy resolution of 110 μeV and those at 15 μeV are plotted in Fig. 2a and b, respectively. The Γ values of LZ2 at 110 μeV have profiles that are rather independent of Q^2, and have non-zero intercepts at $Q = 0$. These profiles also appear to have a tendency to increase in the high-Q region. These characteristics of the profiles imply that the observed motions are diffusive motions within a confined volume (Bee 1988). The Γ values of other Lorentzians also have non-zero intercepts at $Q = 0$: the Γ values of LZ1 at 110 μeV are between 0.01 and 0.04 meV, and those of LZ2 at 15 μeV are around 0.05 meV, though the values of LZ1 at 15 μeV go close to zero. The non-zero intercept at $Q = 0$ is also an indication of diffusive motions within a confined volume. These Γ values, however, show asymptotic behavior to the high-Q region. This behavior is one of the characteristics of jump diffusion (Bee 1988). While in the lower-Q region where the long range motions are dominant, the motions observed are considered to be continuous, in the high-Q region where local motions are important, elemental steps that each proton undergoes become "visible". The average values of the plateau regions in LZ2 at 110 μeV and the asymptotic values of LZ2 at 15 μeV, LZ1 at 110 and 15 μeV are plotted as guide-lines for the eye in Fig. 2. Table 1 summarizes these Γ values and the corresponding correlation times, τ. The motions detected by LZ2 cover the range of the correlation times of the order of ps while those by LZ1 cover the range of the order of ps to tens of ps. The motions detected from the measurements at 110 and 15 μeV cover similar but somewhat different ranges, corresponding to the different energy resolutions. These values show that not only G-actin tends to have smaller correlation times, but also increasing hydration decreases the correlation time. These results indicate that G-actin fluctuates more rapidly than F-actin, and that more hydration induces more rapid fluctuations.

Analysis of elastic incoherent structure factors

The elastic incoherent structure factor (EISF), $A_0(Q)$ in Eq. 1, contains information on the geometry of the

Table 1 Summary of the Γ values and the corresponding correlation time, τ

		Hydration ratio	F-actin		G-actin	
			Γ (meV)	τ (ps)	Γ (meV)	τ (ps)
LZ2 (110 μeV)	Plateau value	0.4	0.27	2.4	0.27	2.4
		1.0	0.36	1.8	0.45	1.5
LZ1 (110 μeV)	Asymptotic value	0.4	0.029	23	0.046	14
		1.0	0.066	10	0.094	7.0
LZ2 (15 μeV)	Asymptotic value	0.4	0.15	4.4	0.13	5.1
		1.0	0.17	3.9	0.18	3.7
LZ1 (15 μeV)	Asymptotic value	0.4	0.017	39	0.016	41
		1.0	0.022	30	0.028	24

motions. The EISF was thus extracted to characterize the geometry of the motions observed. The experimental EISF can be calculated as the ratio of the elastic intensity to the sum of the elastic intensity and the quasielastic intensity. Figure 3 shows the EISF curves obtained. These curves can be fit with the equations describing various models of the motions, such as the diffusive motions within a sphere, and the local jumping motions between distinct sites. Here we employed a model representing the diffusive motions within a sphere, in which each atom diffuses freely inside an impermeable sphere of radius a, as suggested by the Q-dependences of the Γ values. This model is described by the equation, $(3j_1(Qa)/Qa)^2$, where j_1 denotes the spherical Bessel function of the first kind of order 1 (Volino and Dianoux 1980). Since the QENS spectra were fit with two Lorentzians, the EISF curves containing two diffusive motions within distinct spheres were employed. The curves were described as:

$$\mathrm{EISF}(Q) = p_0 + p_1(3j_1(Qa_1)/Qa_1)^2 + p_2(3j_1(Qa_2)/Qa_2)^2, \quad (2)$$

where p_0 denotes the fraction of the contribution from the "immobile" protons, the motions of which are outside the energy window of the measurements, p_1 and p_2 are the fractions of the contributions from the diffusive motions within a sphere of radius a_1 and those within a sphere of radius a_2, respectively, and $p_0 + p_1 + p_2 = 1$.

The best-fit curves of the model by using Eq. 2 are also shown in Fig. 3. The fits are in good agreement with the data. Table 2 summarizes the parameter values obtained. Because of high non-linearity of the fitting equation and statistics of the data points, the errors of the parameters propagated through the fits were rather large, particularly for the curves from the measurements at 15 μeV. Nevertheless, clear tendencies of the parameter values were observed. The effects of increasing hydration were primarily on the fractions of the contributions from the various motions, p_0, p_1, and p_2. These fractions correspond to

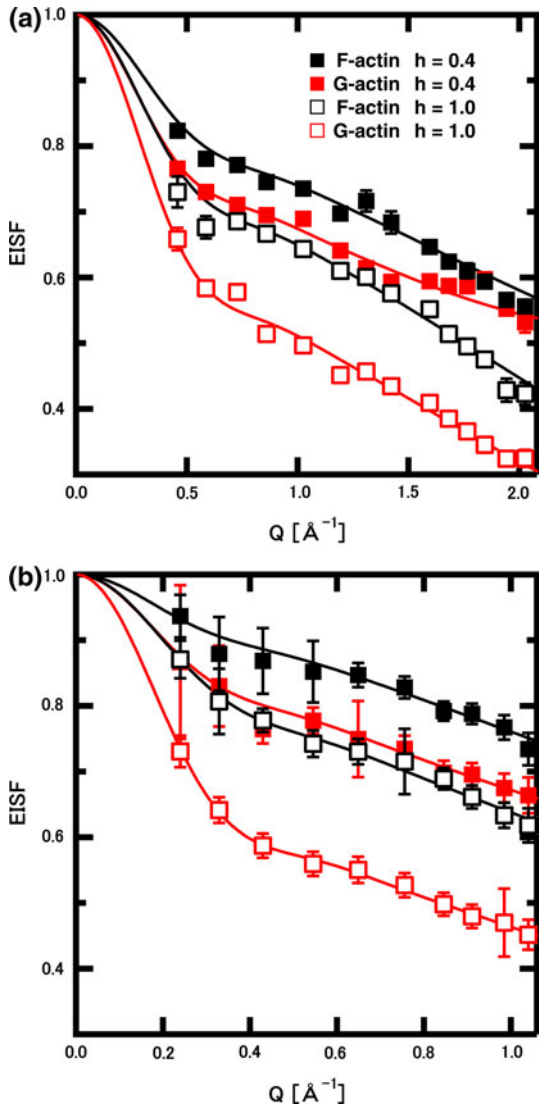

Fig. 3 The EISF curves estimated from the fit with Eq. 2 containing the two Lorentzians. **a** The curves from the measurements at ΔE of 110 μeV and **b** the curves from the measurements at ΔE of 15 μeV are shown. The *error bars* of the data points are within *symbols* if not shown

Table 2 Summary of the best-fit parameter values of the EISF curves by the models consisting of two diffusional motions within a confined sphere

		F-actin		G-actin	
		$h = 0.4$	$h = 1.0$	$h = 0.4$	$h = 1.0$
$\Delta E = 110$ μeV	p_0	0.41 (0.06)	0.16 (0.22)	0.51 (0.02)	0.14 (0.08)
	p_1	0.19 (0.01)	0.26 (0.02)	0.24 (0.01)	0.40 (0.01)
	a_1 (Å)	5.7 (1.5)	5.9 (2.2)	6.3 (0.55)	5.9 (0.2)
	p_2	0.4 (0.06)	0.58 (0.22)	0.25 (0.02)	0.46 (0.08)
	a_2 (Å)	1.0 (0.1)	0.91 (0.23)	1.4 (0.1)	1.0 (0.2)
$\Delta E = 15$ μeV	p_0	0.60 (0.59)	0.48 (0.48)	0.58 (0.30)	0.34 (0.34)
	p_1	0.076 (0.069)	0.18 (0.05)	0.16 (0.08)	0.37 (0.04)
	a_1 (Å)	10 (9.0)	9.0 (0.33)	9.9 (6.9)	9.4 (0.96)
	p_2	0.33 (0.60)	0.34 (0.48)	0.27 (0.31)	0.28 (0.34)
	a_2 (Å)	1.8 (2.4)	1.8 (2.4)	2.2 (2.1)	2.0 (1.8)

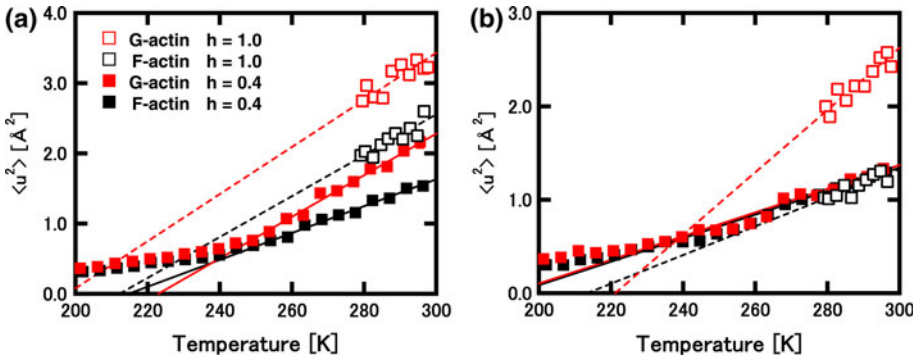

Fig. 4 The mean square displacements, $<u^2>$, of F-actin and G-actin as a function of temperature. The values estimated from **a** the Guinier region and **b** the high-Q region are plotted. The data above 200 K are shown. *Filled squares* in *black* and *open squares* in *black* denote the data of F-actin at $h = 0.4$ and at $h = 1.0$, respectively. *Filled squares* in *red* and *open squares* in *red* denote those of G-actin at $h = 0.4$ and at $h = 1.0$, respectively. The *error bars* are within *symbols*. *Solid* and *dashed lines* represent the fits to the data above 280 K. Note that the data at $h = 0.4$ are reproduction shown in the previous report (Fujiwara et al. 2008). These data are shown as a standard for the comparison with the data at $h = 1.0$

the relative populations of the atoms that are "immobile", those undergoing the diffusive motions within larger spheres, and those undergoing the diffusive motions within smaller spheres, respectively, within the protein. The population of the immobile atoms (p_0) was lowered by increasing hydration, indicating that more atoms are observable in the energy window of the measurements. The populations of the atoms undergoing the diffusive motions within larger spheres (p_1) and smaller spheres (p_2) increase correspondingly. The degree of increases in p_1 was more significant in G-actin, compared to F-actin. This indicates that in G-actin, the population of the atoms undergoing diffusive motions with large amplitudes increases significantly with increasing hydration, compared to F-actin. The difference in the effects of increasing hydration between F-actin and G-actin lies in this difference in the populations.

EINS measurements

We also carried out EINS measurements to see how the hydration affects the mean square displacements, $<u^2>$. Figure 4 shows temperature dependences of $<u^2>$ of F-actin at $h = 0.4$ and 1.0, and G-actin at $h = 0.4$ and 1.0, estimated from (a) the Guinier regions and (b) the high-Q regions of the EINS spectra. The EINS measurements on the samples at $h = 1.0$ were done only above 275 K to avoid possible ice formation. Because of this, analysis based on the three energy states could not be applied as was done for the samples at $h = 0.4$, the measurements of which were done in the temperature range between 20 and 300 K (Fujiwara et al. 2008). Slopes of the curves can still be a measure of flexibility (Zaccai 2000). Figure 4a shows clearly that the curve of F-actin at $h = 1.0$ has a steeper slope than that of F-actin at $h = 0.4$, and the curves of

G-actin have similar tendency though the changes in the slope are less significant. The values of the effective force constant, k', which is inversely related to the flexibility of the protein, were estimated from the slopes of these curves between 280 and 300 K, $d<u^2>/dT$, by the equation, $k' = k_B/(d<u^2>/dT)$ where k_B is the Boltzmann constant (Zaccai 2000). The values obtained are summarized in Table 3. The values of k' clearly demonstrate that G-actin is more flexible than F-actin as shown in the previous report (Fujiwara et al. 2008). Comparison of the k' values at $h = 0.4$ and 1.0 shows that with increasing hydration, the overall flexibility of both F-actin and G-actin increases.

Figure 4b shows the temperature dependencies of $<u^2>$ from the high-Q region. Another difference between F-actin and G-actin was observed here. While the $<u^2>$ values of F-actin at $h = 1.0$ were similar to those of F-actin at $h = 0.4$ and G-actin at $h = 0.4$, the $<u^2>$ values of G-actin at $h = 1.0$ are significantly larger than those of G-actin at $h = 0.4$ and F-actin. Since $<u^2>$ from the high-Q region correspond to motions with smaller amplitudes (Réat et al. 1997; Lehnert et al. 1998; Gabel et al. 2004), these results imply that F-actin contains a region in which the amplitudes of the motions stay similar when the hydration increases, while in G-actin a fraction of such a "core" region decreases and changes into "flexible" regions with increasing hydration. The k' values from these curves are also summarized in Table 3. Significant decrease in k' of G-actin to a value similar to that obtained from the $<u^2>$ curve estimated from the Guinier region implies that in G-actin, the whole molecule increases its flexibility with increasing hydration.

Discussion

We have characterized the internal dynamics of F-actin and G-actin from QENS and EINS measurements. Analysis of the QENS spectra showed that there are, on average, two distinct motions. The analysis employed here was "phenomenological fits", in which a sum of (in principle) an infinite number of Lorentzians was approximated by a sum of two Lorentzians. The motions detected were thus averaged motions. The correlation times of the motions detected range from the order of ps to the order of tens of ps. The rather large range of the correlation times implies that the observed motions have a broad distribution in rates and amplitudes. Analysis of the EISF curves provided the geometrical characteristics of the observed motions. Here the model employed to fit the EISF curves was one containing two diffusive motions within a sphere with distinct radii (and the "immobile" atoms). The radii of the spheres reflect the broad distribution, ranging from $\sim$1 to $\sim$10 Å.

Although these motions were averaged motions and should not be ascribed to any specific motions, this approach is still useful in observing how the different states affect the dynamics. Differences in the QENS spectra between samples with different degrees of hydration were detected as well as the differences between F-actin and G-actin. The samples at $h = 1.0$ contain extra amounts of D_2O that could induce changes in the spectra. However, the contribution of D_2O to neutron scattering intensity, calculated from the atomic composition of the actin molecule and hydration ratio, is at most 5% ($\sim$2% for the samples at $h = 0.4$). The difference spectra between the samples at $h = 1.0$ and $h = 0.4$ after normalizing by the amount of the actin molecules in the samples have values far larger than this relative contribution of D_2O (about 45% on average in a quasielastic regime). Furthermore, the changes in the spectra with increasing hydration appear as the decrease in the elastic peak and the increase in the quasielastic scattering (the data not shown). Such changes would not be the result of the addition of extra amounts of solvent, but of changes in the dynamics. Thus, the main contribution to the changes in the QENS spectra is assigned to the changes in the internal dynamics of the actin molecules.

The spectra measured here are dominated by "*incoherent*" neutron scattering, arising from the motions of the atoms contributing individually. The overall geometry of F-actin or the anisotropy induced by interactions between F-actin, such as the bundle formation occurring at high concentrations of F-actin, do not distort the spectra, unless such macroscopic geometry affects local dynamics on a picosecond time scale and an Ångstrom length scale. Since the bundle formation occurs through long-range electrostatic interactions between polyelectrolytes (Tang and Janmey 1996) rather than through specific interactions between the actin molecules, it is unlikely that the actin molecules in the adjacent filaments interact so closely that significant changes in the dynamics of the interacting regions occur. In addition, no peak was observed in the X-ray diffraction patterns of the F-actin powders (not shown) at the position corresponding to the Bragg spacing larger than 69 Å, which is an indication of the formation of the bundles or the paracrystals (Spencer 1969; Matsudaira et al. 1983). Contribution of the anisotropy due to the

Table 3 Summary of the effective force constant k′ [N/m], estimated from the Guinier regions and the high-Q regions of the EINS curves

	F-actin		G-actin	
	$h = 0.4$	$h = 1.0$	$h = 0.4$	$h = 1.0$
Guinier region	0.14 (0.02)	0.095 (0.007)	0.094 (0.011)	0.082 (0.007)
High-Q region	0.22 (0.03)	0.18 (0.02)	0.22 (0.04)	0.083 (0.004)

bundle formation in F-actin is therefore considered not to affect the dynamics observed here.

The analysis of the EISF curves showed that geometrical characteristics of each observed motion are not affected by the structural states or by increasing hydration. This implies that the environment around "averaged" protons, the motions of which are represented by each term in Eq. 2, does not change. The changes occur in relative populations of the atoms undergoing the motions with distinct geometrical characteristics. Increasing hydration affects these changes differently between F-actin and G-actin. In G-actin, the population of the atoms undergoing the motions confined in a larger volume increases significantly compared to F-actin. Since the actin molecule consists of a rigid core and flexible loop regions as observed in the previous report (Fujiwara et al. 2008), this implies that in G-actin, more surface loops become flexible so that they undergo diffusive motions of large amplitude. In F-actin, on the other hand, the molecular interactions that keep the polymerized state suppress the large motions of the surface loops involved with polymerization so that the population of atoms undergoing the large motions increases to a lesser degree. Note here that although the geometry of the motions is similar between G-actin and F-actin, the rates of the fluctuations are different: G-actin fluctuates more rapidly than F-actin as observed by the correlation times. This difference could reflect the difference in the dynamics of water molecules around G-actin and F-actin. Indeed, a close relationship between the internal dynamics of the protein and the dynamics of hydration water has been pointed out (for reviews, for example, Smith 1991; Gabel et al. 2002; Doster and Settles 2005). However, the present data do not enable one to draw conclusions about the origins of the difference in the dynamics because it is not possible to measure the dynamics of water from the samples employed in the present study.

The EINS experiments provided the concerted results. Variations in the $<u^2>$ and k' values showed that F-actin contains the core region, which keeps motions with similar amplitudes with increasing hydration, and the flexible regions, which undergo motions with large amplitudes and becomes more flexible with increasing hydration. In particular, the significant decrease in k' from the Guinier region couple with the rather small decrease in k' from the high-Q region suggests that the increase in the overall flexibility arises mainly from the increase in the flexibility of the flexible regions in F-actin. In G-actin, on the other hand, the increase in the fraction of the flexible region induces a further increase in the overall flexibility. These results are consistent with the interpretation that the differences in the effects of increasing hydration on F-actin and G-actin arise from differences in the surface loop regions.

Here we have shown from the QENS and EINS measurements that the behavior related to the increase in hydration is different in G-actin and F-actin. The increase in the fraction of the flexible regions in G-actin with increasing hydration implies that the surface loops of the actin molecule have a distribution of flexibility. Such a distribution of flexibility might be related to the mechanism of molecular recognition between the interacting regions in the actin molecules, which should occur in the initiating stages of polymerization. The behavior of F-actin suggests that the loop regions that are not involved with the interactions between the actin molecules are the most flexible. Such flexible regions might be the origin of the multifunctions of F-actin because such regions could adapt various conformations that enable F-actin to interact with various proteins.

Acknowledgments We thank Dr. Tomoki Aihara for his help in sample preparation, and Dr. Lambert van Eijck for his help during the experiments with IN5 and IN16. We also thank Prof. Giuseppe Zaccai for his help in conducting the experiments. The X-ray diffraction measurements were done under the approval of the RIKEN Beam-Line Committee (Proposal No. 2010015). This study was supported in part by Grant-in-Aid for Scientific Research on Innovative Areas from the Ministry of Education, Culture, Sports, Science and Technology (SF).

References

Astbury WT, Perry SV, Reed R, Spark LC (1947) An electron microscope and X-ray study of actin. Biochim Biophys Acta 1:379–392

Bastos M, Castro V, Mrevlishvili G, Teixeira J (2004) Hydration of ds-DNA and ss-DNA by neutron quasielastic scattering. Biophys J 86:3822–3827

Bee M (1988) Quasielastic neutron scattering, principles and applications in solid state chemistry, biology and Materials Science. Adam Hilger, Bristol and Philadelphia

Bellissent-Funel MC, Teixeira J, Bradley KF, Chen SH (1992) Dynamics of hydration water in protein. J Phys I 2:995–1001

Bon C, Dianoux J, Ferrand M, Lehmann MS (2002) A model for water motion in crystals of lysozyme based on an incoherent quasielastic neutron-scattering study. Biophys J 83:1578–1588

Bu Z, Neumann DA, Lee SH, Brown CM, Engelman DM, Han CC (2000) A view of dynamics changes in the molten globule-native folding step by quasielastic neutron scattering. J Mol Biol 301:525–536

Bu Z, Cook J, Callaway DJE (2001) Dynamic regimes and correlated structural dynamics in native and denatured alpha-lactalbumin. J Mol Biol 312:865–873

Carlier MF, Pantaloni D (1997) Control of actin dynamics in cell motility. J Mol Biol 269:459–467

Caronna C, Natali F, Cupane A (2005) Incoherent elastic and quasielastic neutron scattering investigation of hemoglobin dynamics. Biophys Chem 116:219–225

De Francesco A, Marconi M, Cinelli S, Onori G, Paciaroni A (2004) Picosecond internal dynamics of lysozyme as affected by thermal unfolding in nonaqueous environment. Biophys J 86:480–487

Dellerue S, Bellissent-Funel MC (2000) Relaxational dynamics of water molecules at protein surface. Chem Phys 258:315–325

Doster W, Cusack S, Petry W (1989) Dynamical transition of myoglobin revealed by inelastic neutron scattering. Nature 337:754–756

Doster W, Settles M (2005) Protein-water displacement distributions. Biochem Biophys Acta 1749:173–186

Fitter J, Lechner RE, Büldt G, Dencher NA (1996) Internal molecular motions of bacteriorhodopsin: hydration-induced flexibility studied by quasielastic incoherent neutron scattering using oriented purple membranes. Proc Natl Acad Sci USA 93:7600–7605

Fitter J, Ernst OP, Hauß T, Lechner RE, Hofmann KP, Dencher NA (1998) Molecular motions and hydration of purple membranes and disk membranes studied by neutron scattering. Eur Biophys J 27:638–645

Fitter J (1999) The temperature dependence of internal molecular motions in hydrated dry α-amylase: the role of hydration water in the dynamical transition of proteins. Biophys J 76:1034–1042

Fitter J (2003) A measure of conformational entropy change during thermal protein unfolding using neutron spectroscopy. Biophys J 84:3924–3930

Fujisawa T, Inoue K, Oka T, Iwamoto H, Uruga T, Kumasaka T, Inoko Y, Yagi N, Yamamoto M, Ueki T (2000) Small-angle X-ray scattering station at the SPring-8 RIKEN beamline. J Appl Cryst 33:797–800

Fujiwara S, Plazanet M, Matsumoto F, Oda T (2008) Difference in internal dynamics of actin under different structural states detected by neutron scattering. Biophys J 94:4880–4889

Gabel F, Weik M, Doctor BP, Saxena A, Founier D, Brochier L, Renault F, Masson P, Silman I, Zaccai G (2004) The influence of solvent composition on global dynamics of human butyrylcholinesterase powders: a neutron scattering study. Biophys J 86:3152–3165

Gabel F, Bicout D, Lehnert U, Tehei M, Weik M, Zaccai G (2002) Proteins dynamics studied by neutron scattering. Q Rev Biophys 35:327–367

Gasper AM, Appavou MS, Busch S, Unruh T, Doster W (2008) Dynamics of well-folded and natively disordered proteins in solution: a time-of-flight neutron scattering study. Eur Biophys J 37:573–582

Guinier A, Fournet G (1955) Small-Angle Scattering of X-rays. Wiley, London; Chapman and Hall, New York

Isambert H, Venier P, Maggs AC, Fattoum A, Kassab R, Pantaloni D, Carlier MF (1995) Flexibility of actin filaments derived from thermal fluctuations Effect of bound nucleotide, phalloidin, and muscle regulatory proteins. J Biol Chem 270:11437–11444

Ishiwata S, Fujime S (1972) Effect of calcium ions on the flexibility of reconstituted thin filaments of muscle studied by quasielastic scattering of laser light. J Mol Biol 68:511–522

Janmey PA, Hvidt S, Oster GF, Lamb J, Stossel TP, Hartwig JH (1990) Effect of ATP on actin filament stiffness. Nature 347:95–99

Jasnin M, Moulin M, Haertlein M, Zaccai G, Tehei M (2008) In vivo measurement of internal and global macromolecular motions in Escherichia coli. Biophys J 95:857–864

Köper I, Combet S, Petry W, Bellissent-Funel MC (2008) Dynamics of C-phycocyanin in various deuterated trehalose/water environments measured by quasielastic and elastic neutron scattering. Eur Biophys J 37:739–748

LAMP, the Large Array Manipulation Program. http://www.ill.fr/data_treat/lamp/lamp.html

Lehnert U, Réat V, Weik M, Zaccai G, Pfister C (1998) Thermal motions in bacteriorhodopsin at different hydration levels studied by neutron scattering: correlation with kinetics and light-induced conformational changes. Biophys J 75:1945–1952

Matsudaira P, Mandelkow E, Renner W, Hesterberg LK, Weber K (1983) Role of fimbrin and villin in determining the interfilament distances of actin bundles. Nature 301:209–214

Matsudaira P, Bordas J, Koch MHJ (1987) Synchrotron X-ray diffraction studies of actin structure during polymerization. Proc Natl Acad Sci USA 84:3151–3155

Orlova A, Egelman EH (1993) A conformational change in the actin subunit can change the flexibility of the actin filament. J Mol Biol 232:334–341

Otterbein LR, Graceffa P, Dominguez R (2001) The crystal structure of uncomplexed actin in the ADP state. Science 293:708–711

Paciaroni A, Stroppolo ME, Arcangeli C, Bizzarri A, Cannistraro S (1999) Incoherent neutron scattering of copper azurin: a comparison with molecular dynamics simulation results. Eur Biophys J 28:447–456

Pérez J, Zanotti JM, Durand D (1999) Evolution of the internal dynamics of two globular proteins from dry powder to solution. Biophys J 77:454–469

Pieper J, Hauss T, Buchsteiner A, Baczyński K, Adamiak K, Lechner RE, Renger G (2007) Temperature- and hydration-dependent protein dynamics in photosystem II of green plants studied by quasielastic neutron scattering. Biochemistry 46:11398–11409

Pieper J, Hauß T, Buchsteiner A, Renger G (2008a) The effect of hydration on protein flexibility in photosystem II of green plants studied by quasielastic neutron scattering. Eur Biophys J 37:657–663

Pieper J, Buchsteiner A, Dencher NA, Lechner RE, Hauβ T (2008b) Transient protein softening during the working cycle of a molecular machine. Phys Rev Let 100:228103-1–228103-4

Pollard TD, Blanchoin L, Mullins RD (2000) Molecular mechanisms controlling actin filament dynamics in nonmuscle cells. Annu Rev Biophys Biomol Struct 29:545–576

Réat V, Zaccai G, Ferrand M, Pfister C (1997) Functional dynamics in purple membrane. In: Cusack S, Büttner H, Ferrand M, Langan P, Timmins P (eds) Biological macromolecular dynamics. Academic Press, New York, pp 117–122

Rebello CA, Ludescher RD (1998) Influence of tightly bound Mg^{2+} and Ca^{2+}, Nucleotides, and phalloidin on the microsecond torsional flexibility of F-actin. Biochemistry 37:14529–14538

Receveur V, Calmetes P, Smith JC, Desmadril M, Coddens G, Durand D (1997) Picosecond dynamical changes on denaturation of yeast phosphoglycerate kinase revealed by quasielastic neutron scattering. Proteins 28:380–387

Rould MA, Wan Q, Joel PB, Lowey S, Trybus KM (2006) Crystal structures of expressed non-polymerizable monomeric actin in the ADP and ATP states. J Biol Chem 281:31909–31919

Smith JC (1991) Protein dynamics: comparison of simulations with inelastic neutron scattering experiments. Q Rev Biophys 24:227–291

Spencer M (1969) Low-angle X-ray diffraction from concentrated sols of F-actin. Nature 223:1361–1362

Spudich JA, Watt S (1971) The regulation of rabbit skeletal muscle contraction 1. Biochemical studies of the interaction of the tropomyosin-troponin complex with actin and the proteolytic fragments of myosin. J Biol Chem 246:4866–4871

Stadler AM, Digel I, Artmann GM, Embs JP, Zaccai G, Büldt G (2008) Hemoglobin dynamics in red blood cells: correlation to body temperature. Biophys J 95:5449–5461

Tang JX, Janmey PA (1996) The polyelectrolyte nature of F-actin and the mechanism of actin bundle formation. J Biol Chem 271:8556–8563

Tehei M, Franzetti B, Wood K, Gabel F, Fabiani E, Jasnin M, Zamponi M, Oesterhelt D, Zaccai G, Ginzburg M, Ginzburg B-Z (2007) Neutron scattering reveals extremely slow cell water in a Dead Sea organism. Proc Natl Acad Sci USA 104:766–771

Volino F, Dianoux AJ (1980) Neutron incoherent scattering law for diffusion in a potential of spherical symmetry: general formalism and application to diffusion inside a sphere. Mol Phys 41:271–279

Zaccai G (2000) How soft is a protein? A protein dynamics force constant measured by neutron scattering. Science 288:1604–1607

Zanotti JM, Bellissent-Funel MC, Parello J (1999) Hydration-coupled dynamics in proteins studied by neutron scattering and NMR: the case of the typical EF-hand calcium-binding parvalbumin. Biophys J 76:2390–2411

Zanotti JM, Hervé G, Bellisent-Funel MC (2006) Picosecond dynamics of T and R forms of aspartate transcarbamylase: a neutron scattering study. Biochem Biophys Acta 1764:1527–1535